A Double Bond Between Two Molecules

Shota Kino,[1,7] Shusaku Ukai,[1,7] Norihito Fukui,[1,2] Rie Haruki,[3] Reiji Kumai,[3]* Qian Wang,[6] Satoshi Horike,[4] Quan Manh Phung,[5] Dage Sundholm,[6]* and Hiroshi Shinokubo[1]*

[1] Department of Molecular and Macromolecular Chemistry, Graduate School of Engineering and Integrated Research Consortium on Chemical Sciences (IRCCS), Nagoya University, Furo-cho, Chikusa-ku, Nagoya, Aichi 464-8603, Japan.

[2] PRESTO, Japan Science and Technology Agency (JST), Kawaguchi, Saitama 332-0012, Japan

[3] Photon Factory, Institute of Materials Structure Science, High Energy Accelerator Research Organization (KEK), Tsukuba 305-0801, Japan

[4] Department of Chemistry, Graduate School of Science, Kyoto University, Kitashirakawa Oiwake-cho, Sakyo-ku, Kyoto 606-8502, Japan

[5] Department of Chemistry, Graduate School of Science, Nagoya University, Furo-cho, Chikusa-ku, Nagoya 464-8602, Japan

[6] Department of Chemistry, Faculty of Science, University of Helsinki, FIN-00014 Helsinki, Finland

[7] These authors contributed equally.

*reiji.kumai@kek.jp; sundholm@chem.helsinki.fi; hshino@chembio.nagoya-u.ac.jp

π-Conjugated molecules with one electronic spin often form π-stacked dimers via molecular-orbital interactions between the two unpaired electrons. These interactions are recognized as intermolecular single bonds between two π-conjugated systems. This then raises the question if a double bond between two such molecules is possible. To answer this question, we have synthesized an antiaromatic Ni(II) bis(pentafluorophenyl)norcorrole. Its dimer adopts a face-to-face-stacked structure with an extremely short stacking distance of 2.97 Å. Importantly, an intermolecular double bond does indeed exist in this system and this bond involves four bonding electrons between the two molecules. The bonding electrons were experimentally observed via synchrotron X-ray diffraction analysis and corroborated by theoretical calculations. The intermolecular interaction of the molecular orbitals imparts the stacked dimer with an

aromatic character that is distinctly different from that of its monomer.

Introduction

In numerous natural and synthetic systems, planar aromatic molecules with 4n+2 (n = 0, 1, 2…) π-electrons assemble in a parallel orientation. This phenomenon is called π–π stacking, which is often essential for the creation of biomolecular structures and for the solid-state properties of organic electronic materials.[1–5] The stacking of aromatic molecules is dominated by London dispersion forces, which originate from the electrostatic interactions between instantaneously induced dipole moments of π-electron clouds (Fig. 1a).[6] Consequently, there are no molecular-orbital interactions between two stacked aromatic molecules.[7,8] The interplanar distance between two aromatic π-systems is typically longer than 3.4 Å, which is the sum of the van der Waals radii (1.7 Å) of two carbon atoms. Moreover, aromatic π-conjugated systems typically adopt offset stacking arrangements to reduce the exchange repulsion between the two π-electron clouds.

An exceptional form of π-stacking is that of open-shell π-conjugated molecules, specifically, delocalized π-radicals with 2n+1 (n = 1, 2, 3…) π-electrons.[9–13] These species often form π-stacked dimers, known as π-dimers, which adopt face-to-face stacking structures with short intermolecular distances of less than 3.4 Å (Fig. 1b). Molecular-orbital interactions occur in π-dimers between the two unpaired electrons in the delocalized singly occupied molecular orbitals (SOMO) of the π-radicals. The bonding interactions in π-dimers is sometimes referred to as pancake bonding, which can be defined as a multi-centered single bond between two π-conjugated systems.[14–17]

The existence of multi-centered single bonds between two π-conjugated systems raises the question, if the formation of a double bond between two π-conjugated systems is possible. The concept of double and multiple pancake bonds has been theoretically proposed by Kertesz and co-workers using density-functional-theory (DFT) calculations for π–π stacked structures with short intermolecular distances.[18,19] However, experimental evidence of intermolecular double bonds between closed-shell π-conjugated organic molecules remains elusive. Here, we report

that a multi-centered double bond can be formed in closely π–π stacked (2.97 Å) antiaromatic π-conjugated compounds with 4n (n = 1, 2, 3…) π-electrons (Fig. 1c). The stacking of antiaromatic molecules induces stacked-ring aromaticity due to strong orbital interactions.[20–24] In fact, stacked-ring aromaticity has been demonstrated in stacked antiaromatic porphyrin derivatives, Ni(II) norcorroles.[25–27] However, the nature of the attractive interactions between two antiaromatic molecules remains unclear. In the present article, we demonstrate the existence of two bonding molecular-orbital interactions between two antiaromatic macrocycles in a stacked dimer of *meso*-bis(pentafluorophenyl)norcorrole Ni(II) (**1**).

We have previously reported that Ni(II) norcorroles often adopt π-stacked structures with short interplanar distances (~3.1 Å).[25–27] To achieve even closer π-stacking, we introduced electron-withdrawing pentafluorophenyl substituents to the *meso* positions of the norcorrole unit to mitigate the π-electron repulsions. Consequently, we achieved the formation of an extremely close face-to-face stacked Ni(II) bis(pentafluorophenyl)norcorrole dimer $(\mathbf{1})_2$, and we investigated its structure and properties.

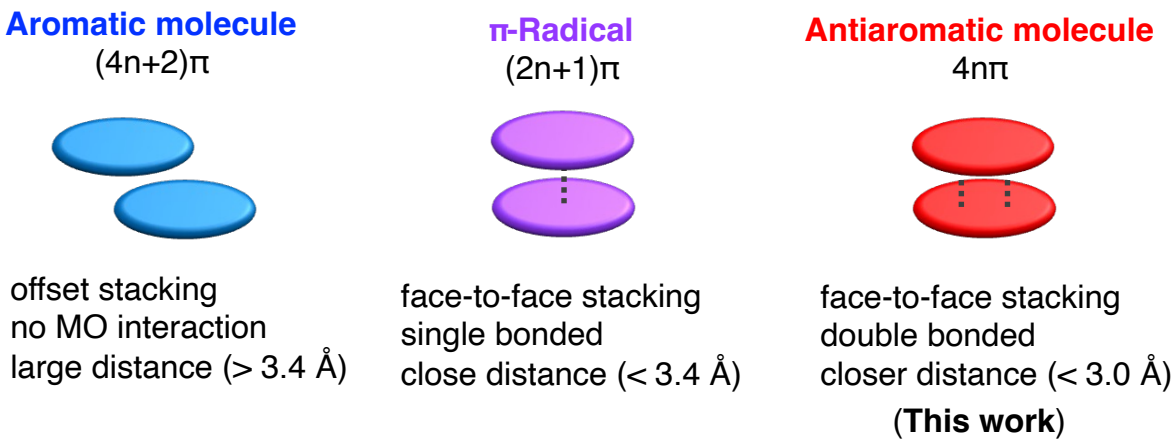

Fig. 1 The orientation of π–stacked π-conjugated molecules. a. The π–π-stacking structure of aromatic molecules. **b.** The π–π-stacking structure of delocalized π-radicals. **c.** The π–π-stacking structure of antiaromatic molecules.

Results and discussion

Synthesis and solid-state structure of *meso*-bis(pentafluorophenyl)norcorrole Ni(II) (1)

Ni(II) norcorrole complex **1** with two pentafluorophenyl groups was prepared via a Ni(0)-

mediated intramolecular reductive C–C bond formation (Fig. 2).[28] Treatment of Ni(II) complex **2** with $Ni(cod)_2$ (4.0 equiv) in the presence of 2,2'-bipyridyl (4.0 equiv) afforded, after quenching the excess amount of the Ni(0) reagent with *p*-chloranil, *meso*-bis(pentafluorophenyl)norcorrole Ni(II) **1** in 60% yield. Norcorrole **1** is relatively stable in the solid state, while a dichloromethane solution of **1** slowly yielded an uncharacterized green insoluble precipitate under ambient conditions.

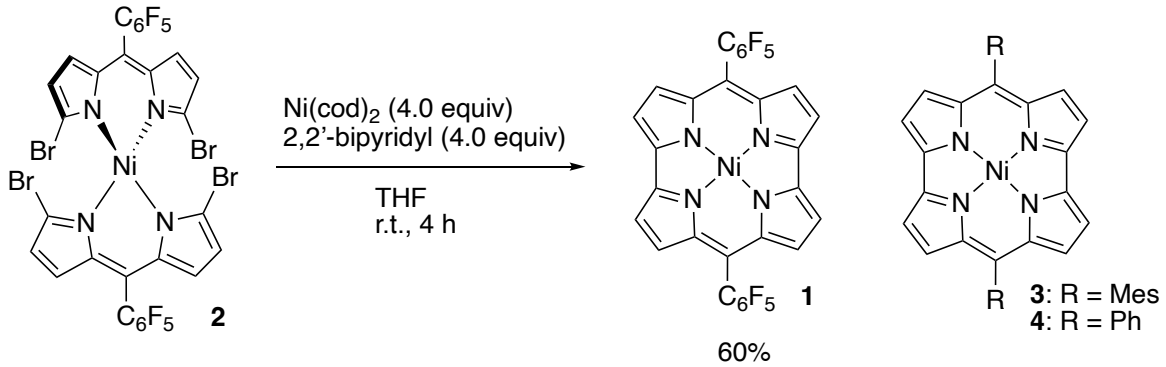

Fig. 2 Synthesis of *meso*-bis(pentafluorophenyl)norcorrole Ni(II) (1).

Following its synthesis, we wanted to examine the solid-state structure of **1** (Fig. 3a). Slow vapor diffusion of pentane into a chloroform solution of **1** provided single crystals suitable for X-ray diffraction analysis. Notably, the stacking distance, defined as the distance between the two mean planes of the four nitrogen atoms of each macrocycle (2.97 Å) is very short compared to typical π-stacking distances (> 3.4 Å) and the closest among stacked norcorroles reported to date.[25–27] Furthermore, the two stacked π systems almost perfectly overlap, with an offset of the two Ni(II) centers of only 0.275 Å and a torsion angle C_{meso}–Ni–Ni'–C'_{meso} of merely 1.5°. This type of face-to-face stacking is rare because the electrostatic repulsion between the π-electron clouds is maximized in a completely overlapping orientation.

The bond-length alternation (BLA) in π-conjugated systems correlates with the extent of the π-electron delocalization. The BLA in the stacked dimer $\mathbf{(1)_2}$ was evaluated based on the harmonic oscillator model of aromaticity (HOMA) values (Fig. 3b).[29] The calculated HOMA value of the norcorrole core (0.74) is substantially higher than that of the non-stacked norcorroles such as Ni(II) dimesitylnorcorrole **3** (0.45).[28] This result indicates that the close π-stacking in $\mathbf{(1)_2}$ results in considerable bond-length equalization due to the effective

delocalization of the π-electrons.

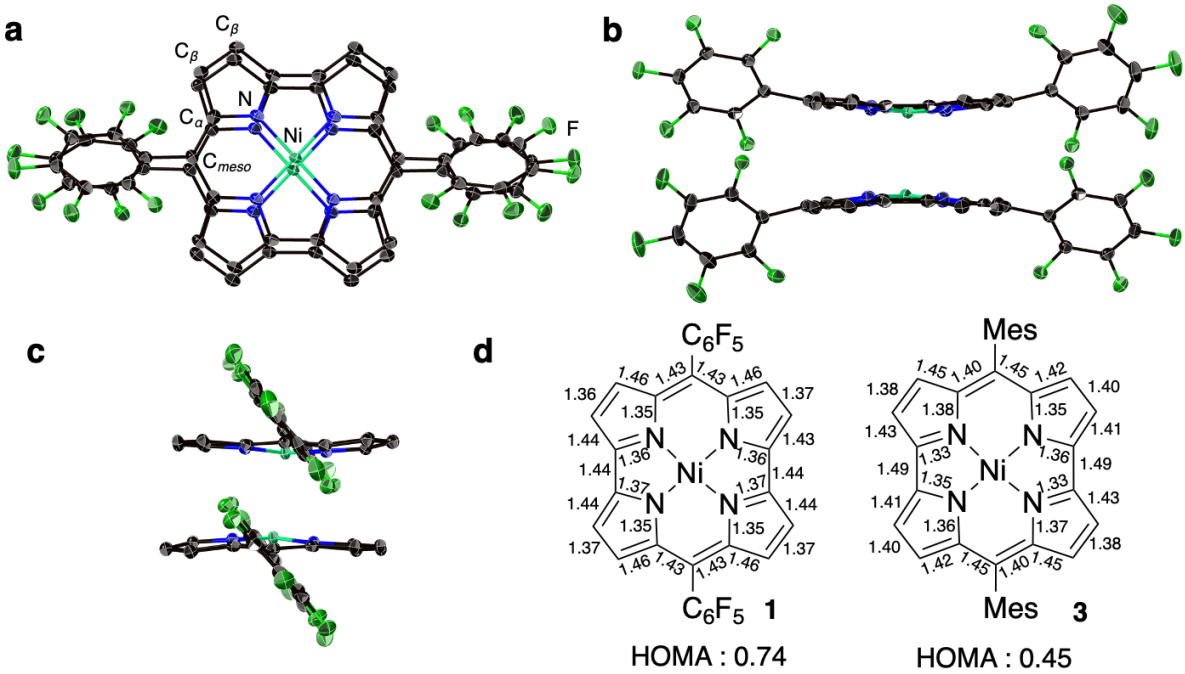

Fig. 3 Solid-state structure of Ni(II) bis(pentafluorophenyl)norcorrole 1. a–c. Solid-state structure of **1** obtained from a single-crystal X-ray diffraction analysis with thermal ellipsoids at 50% probability; all hydrogen atoms are omitted for clarity. **d.** Selected bond lengths and HOMA values of stacked dimer **(1)$_2$** and Ni(II) dimesitylnorcorrole **3**.

Origin of the close π–π stacking

To clarify the origin of the remarkably closely stacked structure, we examined the frontier orbitals of norcorrole monomer **1** and stacked dimer **(1)$_2$** using DFT calculations at the B3LYP/def2-TZVP level (Fig. 4).[30,31] The combination of the two highest occupied molecular orbitals (HOMOs) and the two lowest unoccupied molecular orbitals (LUMOs) of norcorrole **1** generates four frontier molecular orbitals (MOs) in dimer **(1)$_2$**. Notably, the HOMO–1 and HOMO of **(1)$_2$** originate from the in-phase combination of the HOMOs and the in-phase combination of the LUMOs of the norcorrole monomer units, respectively. Four electrons are accommodated in these two bonding MOs, which leads to the formation of two bonding interactions. Consequently, two multi-centered bonds exist between the two norcorrole units and are the origin of the attractive intermolecular interactions in **(1)$_2$**. It seems thus feasible to conclude that the two intermolecular bonding interactions and the mitigated exchange-repulsive

force between the π-electron clouds result in the remarkably close π–π stacked structure of **(1)**$_2$. Moreover, the electron-withdrawing C_6F_5 groups decrease the electrostatic potential on the π-surface of the norcorrole unit (Supplementary Fig. 10).

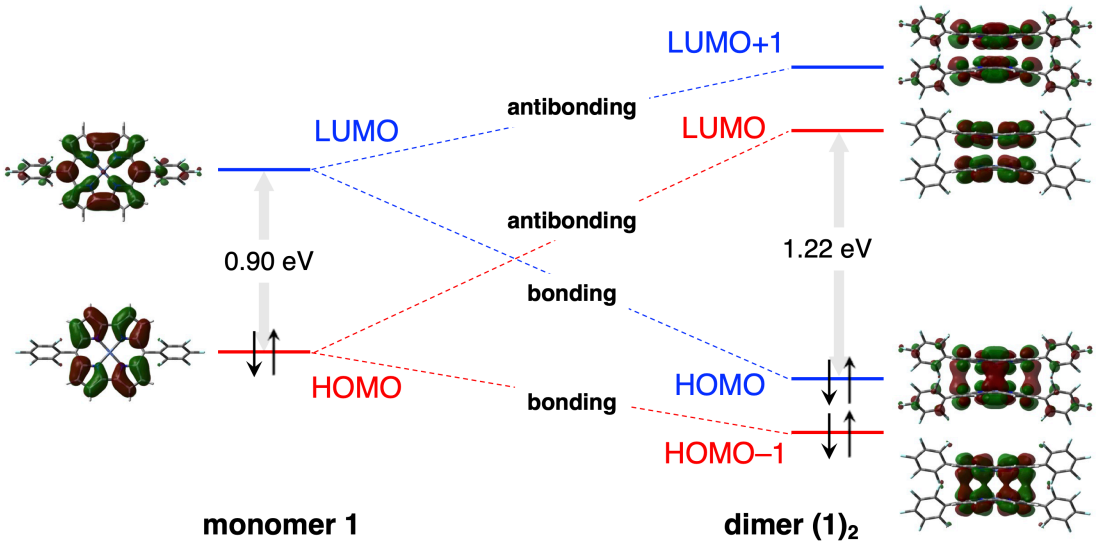

Fig. 4 Frontier molecular orbitals of norcorrole monomer 1 and stacked dimer (1)$_2$. The geometries of **1** and **(1)**$_2$ for single-point calculations were obtained from the crystal structure; all calculations were carried out at the B3LYP/def2-TZVP level.

Electron-density analysis of bonding electrons

The DFT calculations showed that the frontier MOs of the dimer consist of two in-phase combinations of the frontier MOs of the monomer units, thus demonstrating the existence of a multi-centered double bond between the two norcorrole units. Therefore, electrons should exist in the space between the macrocycles to bind the two π-systems together. We therefore attempted to observe these binding electrons via synchrotron X-ray diffraction analysis. The obtained electron-density map indicates the presence of binding electrons between the two nitrogen atoms as well as between the two nickel atoms of the stacked norcorroles (Fig. 5a). There is also some non-negligible electron density present between the two *β*-carbon atoms of the pyrrole subunits (Fig. 5b).

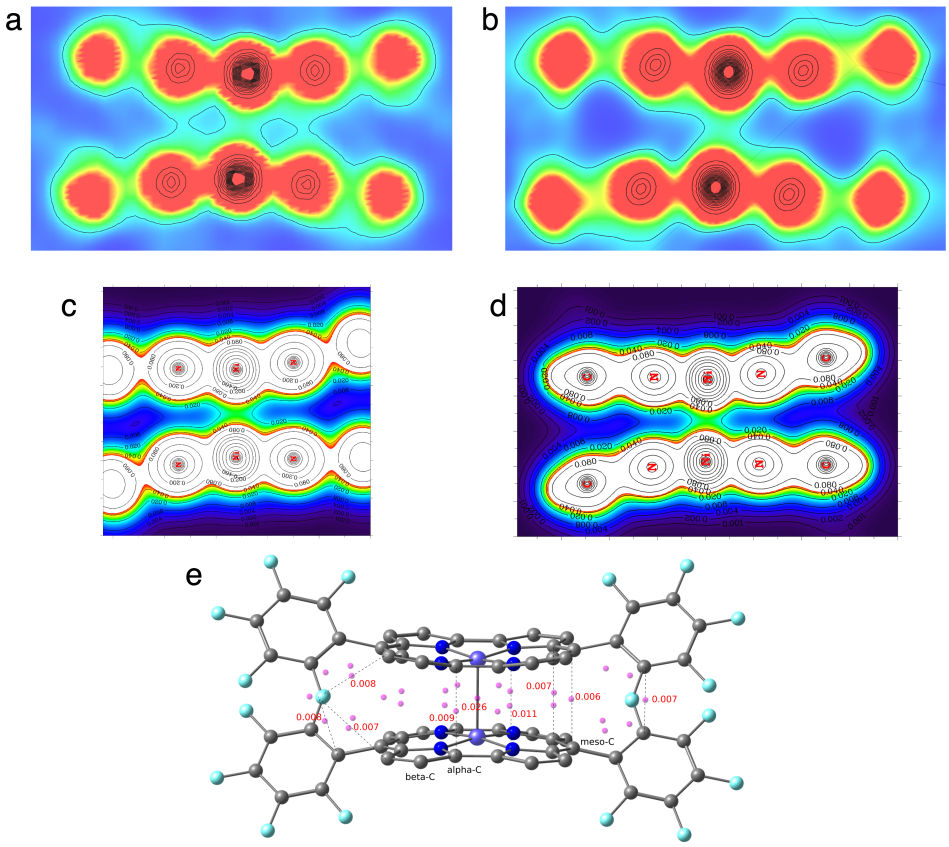

Fig. 5 Analysis of the electron-density distribution of stacked dimer (1)$_2$. a. Experimentally obtained electron-density map in the vertical plane defined by the four nitrogen atoms. **b.** Experimentally obtained electron-density map in the vertical plane defined by four *β*-carbon atoms. **c.** Calculated electron-density map in the vertical plane defined by the four nitrogen atoms. **d.** Calculated electron-density map in the plane defined by the four *β*-carbon atoms; all calculations were carried out at the B3LYP/def2-TZVP level; electron-density range: 0-0.05 electron/bohr^3. **e.** Bond-critical points (BCP) in the region between the two macrocycles of **(1)$_2$**; red numbers represent the electron density at the BCPs.

The electron-density distribution in **(1)$_2$** was also simulated using DFT calculations. The face-to-face stacked structure of **(1)$_2$** was well reproduced using calculations at the B3LYP/def2-TZVP level (Supplementary Fig. 9). To address the dispersion effects between the two norcorrole rings and the C_6F_5 substituents, the semi-empirical dispersion correction D3(BJ) was employed.[32] The calculated electron-density plot of **(1)$_2$** is thus consistent with that obtained experimentally (Figs. 5c and 5d). Notably, we observed electron density between pairs

of atoms belonging to different norcorrole macrocycles, including Ni–Ni, N–N, C_{meso}–C_{meso}, C_{α}–C_{α}, and C_{β}–C_{β}.

To quantitatively assess these pairs of atom-atom interactions in **(1)$_2$**, we determined their bond-critical points (BCPs) and determined the corresponding electron density at the BCPs using the quantum theory of atoms in molecules (QTAIM) approach (Fig 5e).[33,34] We also estimated the interaction energy associated with these interactions.[35] We identified 15 BCPs between the two norcorrole macrocycles and 14 BCPs arising from interactions related to the pentafluorophenyl groups. The electron-density value for the Ni–Ni BCP in **(1)$_2$** (0.026 electron bohr^{-3}) is higher than those for the BCPs between the C–C and N–N pairs (0.006-0.01 electron bohr^{-3}), albeit that the sum of the electron density for these BCPs is substantially larger than that at the Ni–Ni BCP. The Ni–Ni interaction energy in **(1)$_2$** (6.8 kcal mol^{-1}) is also higher than the C–C and N–N interaction-energy values (0.8–1.4 and 2 kcal mol^{-1}, respectively). However, collectively, the total interactions encompassing the 14 pairs of C–C and N–N interactions have a significant cumulative interaction energy of up to 19 kcal mol^{-1}.

NMR spectra of stacked dimer (1)$_2$ in solution

The structure of norcorrole **1** in solution was investigated via nuclear magnetic resonance (NMR) spectroscopy. The ^{1}H NMR spectrum of **1** in $CDCl_3$ (1.0 mM) at room temperature exhibits a broad singlet at δ = 2.5 ppm for the pyrrole protons (Supplementary Fig. 4a). The signal is shifted down-field from 1.7 to 3.7 ppm upon increasing the concentration of **1** (0.5 → 3.5 mM). Based on a nonlinear-curve-regression analysis of the changes in the chemical shifts, the association constant of **1** was determined to be (6.0 ± 0.16) × 10^2 M^{-1} (Supplementary Fig. 4b). This value is substantially higher than that of *meso*-diphenylnorcorrole Ni(II) (**4**; 1.7 × 10 M^{-1}), confirming that the electron-withdrawing C_6F_5 groups facilitate the molecular association of **1** in solution.

The chemical shifts of **1** are also sensitive to temperature. Upon heating a toluene-d_8 solution of **1** (0.51 mM), the pyrrole-proton signals were shifted upfield to –0.4 ppm (Fig. 6a). This remarkable upfield shift of the peaks of **1** can be interpreted in terms of the distinct

antiaromatic nature of monomeric **1** and the electron-withdrawing effect of the pentafluorophenyl groups. The pyrrole-proton signals in the aromatic region are shifted downfield to 6.0–6.7 ppm at lower temperatures (Fig. 6b). The proton signals split into four peaks at 193 K, which is consistent with the slightly displaced face-to-face stacked structure of **(1)$_2$**. The intermolecular double bond between the two monomers holds them in close proximity, even in solution, while the Pauli repulsion between the π-electron clouds is reduced due to the slight displacement of the monomers with respect to each other. The substantial downfield shift of the proton signals in the stacked dimer **(1)$_2$** suggests the establishment of stacked-ring aromaticity (*vide infra*).

This downfield shift of the proton signals in the stacked dimer **(1)$_2$** was confirmed using solid-state ^{1}H NMR measurements. The ^{1}H NMR spectrum of **(1)$_2$** exhibits the pyrrole-proton signals at 7.45 and 3.06 ppm (Fig. 6c) and the presence of a proton peak in the downfield region at 7.45 ppm is evidence of the aromatic nature of **(1)$_2$**. The signal at 3.06 ppm was assigned to the two pyrrole protons above the adjacent norcorrole macrocycle in the crystal-packing structure (Fig. 6d) and the upfield shift is due to the diatropic ring current of the proximal norcorrole dimer.

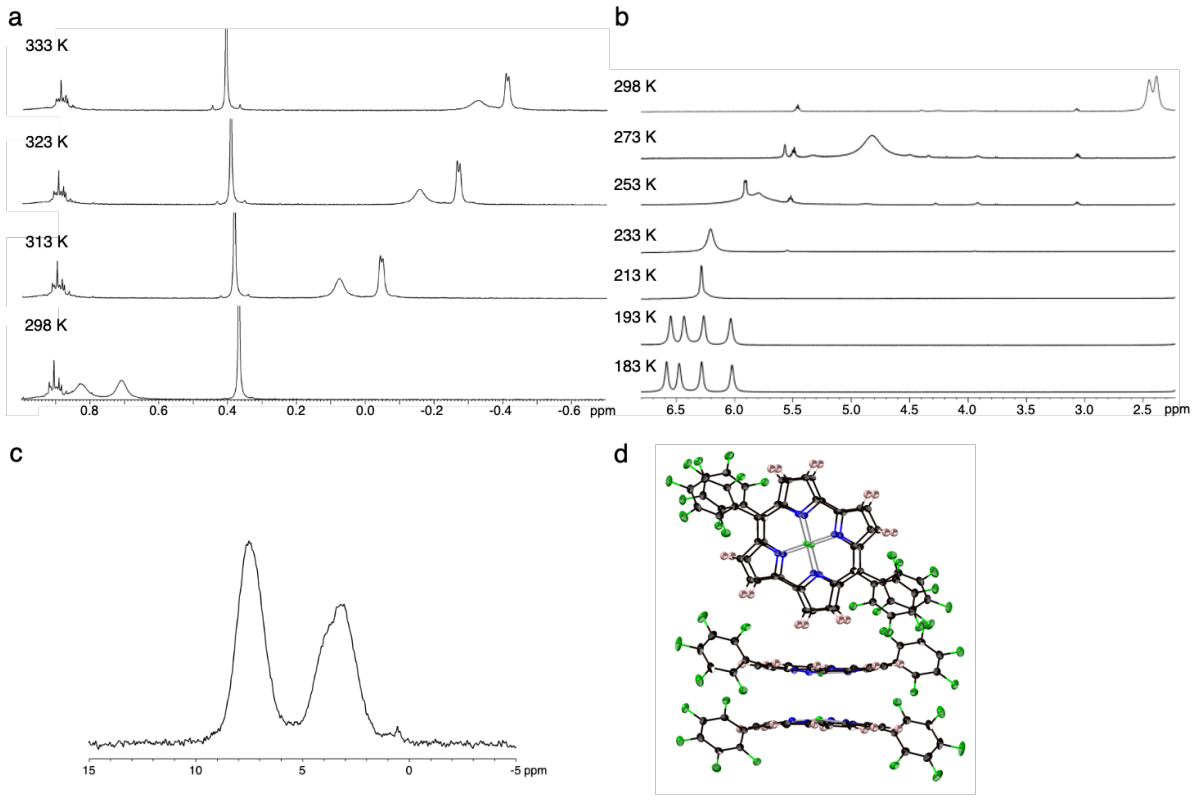

Fig. 6 ^{1}H NMR spectra of 1 in solution and the solid state. a. Temperature-dependent ^{1}H NMR spectra of **1** in toluene-d_8 (0.51 mM) between 298 K and 183 K. **b.** Temperature-dependent ^{1}H NMR spectra of **1** in toluene-d_8 (2.8 mM) between 298 K and 333 K. **c.** Solid-state ^{1}H NMR spectrum of **(1)$_2$**. **d.** Crystal-packing structure of **(1)$_2$**.

Absorption spectra of the stacked dimer (1)$_2$

The electronic-absorption spectra of norcorroles provide insight into their aggregation structure in solution. As the HOMO–LUMO transition of monomeric norcorroles is dipole forbidden, the spectra of norcorrole monomers exhibit weak and broad absorption bands in the near-infrared (NIR) region (Supplementary Fig. 11a). In contrast, the corresponding stacked dimers show distinct absorption bands at ~800 nm because the HOMO–LUMO transition of the norcorrole dimer is dipole allowed (Supplementary Fig. 11c). A solution of norcorrole **1** in dichloromethane (1.0 mM) exhibited a broad peak at 790 nm, the intensity of which significantly increased when the temperature was lowered. The spectral shape at 298 K is similar to the solid-state absorption spectrum of a solid sample of **(1)$_2$**. The intensity of the peak

at 790 nm is about half of that at 440 nm. The spectral features of the face-to-face-stacked dimer **(1)$_2$** were well reproduced using time-dependent (TD) DFT calculations[36] at the CAM-B3LYP[37]/def2-TZVP level. The calculations also show that if **1** had a twisted-stacked structure it would most likely exhibit a weaker absorption band in the NIR range than the one observed (Supplementary Fig. 11b). Based on these findings and the ^{1}H NMR analysis, it seems feasible to conclude that the dominant species of **(1)$_2$** in solution at low temperature is a face-to-face-stacked dimer, indicating that the double-bonding interaction in **(1)$_2$** is sufficiently strong to maintain dimers in solution.

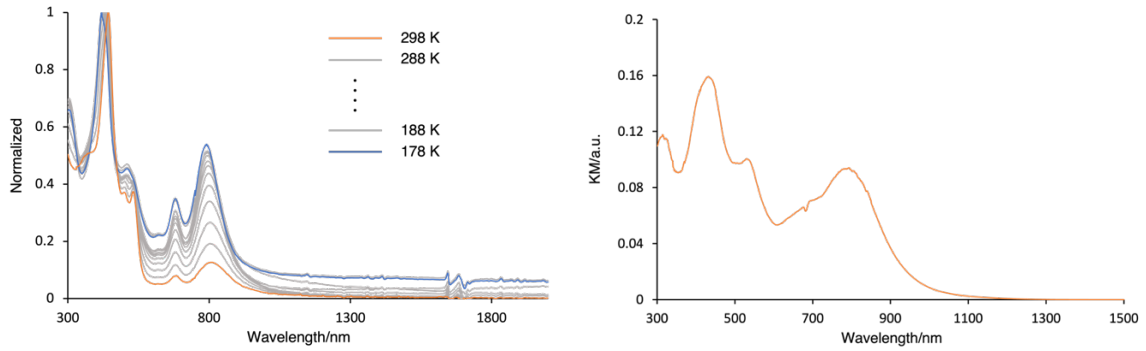

Fig. 7 Absorption spectra of stacked dimer (1)$_2$ a. Temperature-dependent UV/vis/NIR absorption spectra of **1** in CH_2Cl_2 (1.0 mM). **b.** Diffuse reflection UV/vis/NIR absorption spectrum of a solid sample of **(1)$_2$**.

Evaluation of the aromatic nature of the stacked norcorrole dimer (1)$_2$

The aromatic nature of **1** and its stacked dimer **(1)$_2$** was quantified by analyzing the magnetically induced current density (MICD) susceptibility, which was obtained from DFT calculations at the BHLYP[38]/def2-TZVP[31] (LIBXC id = 436)[39] level using the gauge including magnetically induced currents (GIMIC) method[40–44] and visualized with the Paraview program (Fig. 8).[45] Considering that the GIMIC method employs gauge-including atomic orbitals (GIAOs), the MICD has no reference to any gauge origin.[46,47] The MICD was further analyzed by calculating the strength of the MICD susceptibility passing through selected planes that intersect the chemical bonds. The integrated MICD-susceptibility strength around the

molecular rings is also called the ring-current strength expressed in units of nA T^{-1}. An external magnetic field was applied along the Ni–Ni axis of **(1)$_2$** and in the same direction for **1**. The MICD was separated into diatropic and paratropic contributions that were visualized separately using Paraview.[48]

The ring-current profile in Fig. 8d shows that **(1)$_2$** sustains a strong global diatropic ring current of 43.4 nA T^{-1}. The five-membered rings between the pyrrole subunits and Ni sustain a local paratropic ring current of about –7 nA T^{-1}. The separated diatropic and paratropic contributions in Fig. 8e and Fig. 8f show that the central five-membered rings, six-membered rings, and Ni^{2+} species have weak local paratropic MICD vortices. In contrast, the magnetic response of **(1)$_2$** is completely dominated by the global diatropic ring current (Fig. 8e). The strong global ring current of the aromatic dimer splits at the pyrrole rings. The current strength of the outer pathway is 31 nA T^{-1} and the rest of the current takes the inner pathway.

As expected from Hückel's 4n+2 aromaticity rule, norcorrole monomer **1** is antiaromatic. This notion is supported by the MICD plots of **1**, which show a sustained paratropic ring current of –44.7 nA T^{-1} that splits at the pyrrole rings (Supplementary Fig. 12). The strength of the outer pathway is about –12 nA T^{-1} and the rest of the current passes near to the pyrrole nitrogen atoms. The five-membered rings between the pyrrole rings sustain a local paratropic ring current of –4.6 nA T^{-1}. Norcorrole **1** exhibits a weak diatropic ring current of 1.9 nA T^{-1} along the outer edge of the molecule. The MICD calculations demonstrate that the aromaticity of **1** completely changes from strongly antiaromatic to aromatic when **1** forms the closely stacked dimer **(1)$_2$**.

The aromatic nature of **(1)$_2$** is also corroborated by the largely negative nucleus independent chemical shift (NICS)[49] values calculated at the BHLYP/def2-TZVP level. The NICS(1) value calculated 1 Å above the upper norcorrole molecule is –16.5 ppm, while the NICS(–1) value calculated 1 Å below the norcorrole plane between the two molecules is –23.6 ppm (Fig. 8a,8b).

The aromatic nature of **(1)$_2$** can be rationalized by creating an approximation of the MOs using the porphyrin-perimeter model.[50,51] The expansion of the angular part of the MOs gives

rise to orbitals of type σ, π, and δ, with angular quantum numbers of m = 0, 1, 2… For aromatic rings, the Aufbau principle yields well-known magic numbers for 4n+2. Norcorrole monomer **1** has 24 electrons in the conjugated MOs, suggesting that its HOMO shell, according to the perimeter model, is half filled, thus leading to it being antiaromatic. The perimeter model can be extended by equivalence with respect to the reflection plane between the norcorroles, since $\mathbf{(1)_2}$ consists of two norcorrole molecules in a face-to-face orientation. The Aufbau principle then leads to closed shells for the stacked porphyrinoids with magic numbers of 4n.[42] The 48 electrons in the conjugated MOs of $\mathbf{(1)_2}$ close the outermost HOMO shell with an angular quantum number of m = 6 and even parity, thus leading to $\mathbf{(1)_2}$ being aromatic.

In a stacked dimer of weakly interacting antiaromatic macrocycles with a large intermolecular separation, the two outermost MOs remain half filled. Consequently, the dimer is also antiaromatic. In contrast, when the interaction between the two antiaromatic macrocycles is strong, the occupation of the frontier orbitals is reorganized to a closed-shell configuration and the dimer becomes aromatic. Thus, the HOMO shell of dimer $\mathbf{(1)}_2$ with an m quantum number of 6 and even parity, according to the perimeter model, confirms the existence of a double bond between the norcorrole macrocycles.

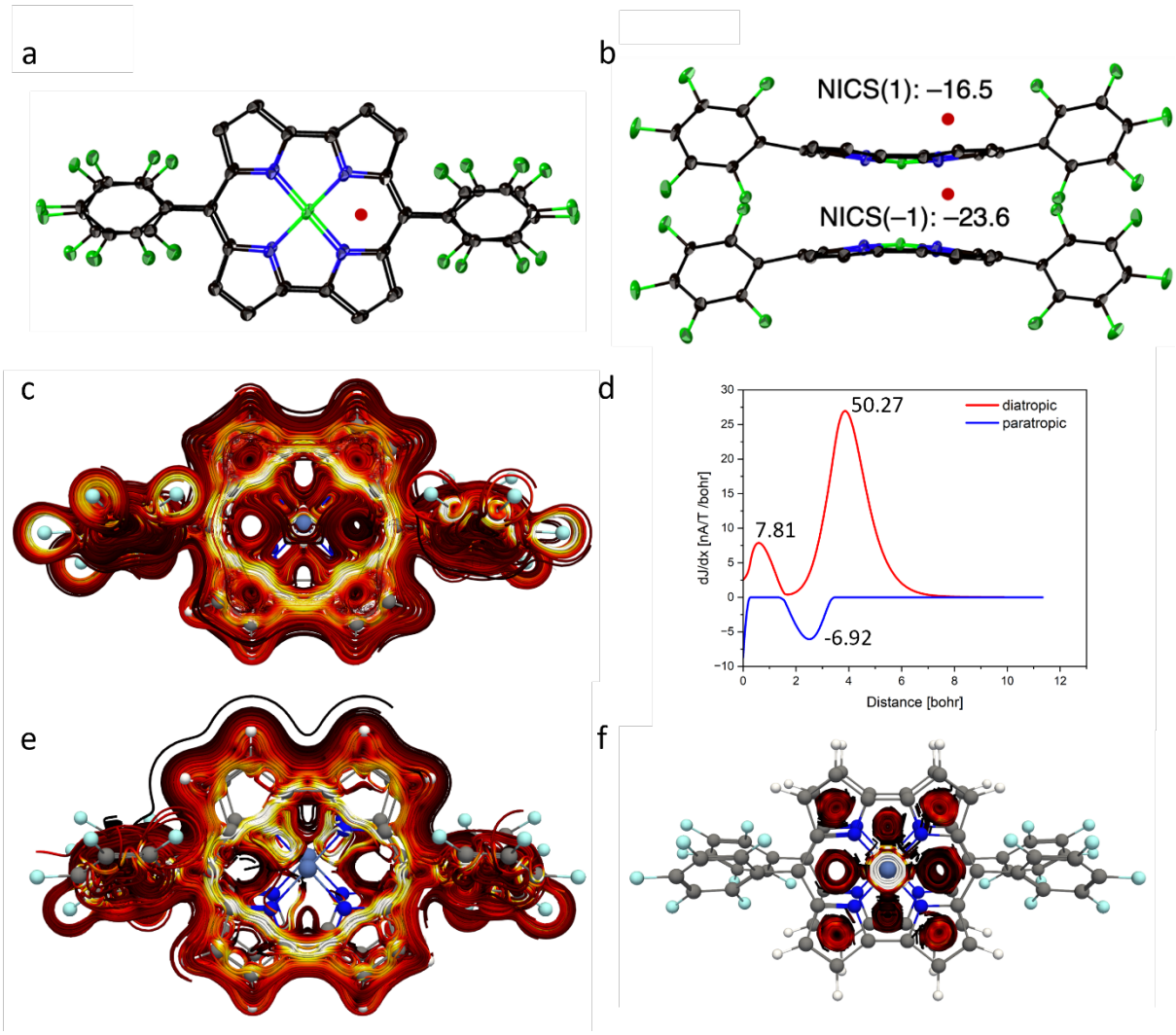

Fig. 8 Evaluation of the aromatic nature of stacked dimer (1)$_2$. a. NICS(1) and NICS(–1) points of **(1)$_2$** seen from above the Ni–Ni axis. **b.** NICS(1) and NICS(–1) values of **(1)$_2$**. **c.** Spaghetti plot of the MICD of **(1)$_2$**. **d.** Profile of the MICD through the plane that cuts the direct bond between the pyrrole rings; MICD-strength values are given in nA T^{-1}. **e.** Diatropic MICD contribution. **f.** Paratropic MICD contribution; the MICD was calculated at the BHLYP/def2-TZVP level; the color scheme in the spaghetti plot corresponds to the strength of the current density, which decreases in the order white > yellow > red > black; all current-density images were created using the Paraview program.

Conclusions

We have synthesized *meso*-bis(pentafluorophenyl)norcorrole Ni(II) (**1**), whose dimer **(1)$_2$** adopts an almost perfectly overlapping face-to-face π-stacked orientation with an extremely

short interplanar distance of < 3.0 Å. The stacked dimer **(1)$_2$** exhibits an aromatic character that is distinctly different from that of monomer **1**, a conclusion that is based on the results of solid-state ^{1}H NMR measurements, UV/vis/NIR spectra, gauge including magnetically induced currents current-density analysis, and ring-current visualization. The origin of the stacking interactions in **(1)$_2$** was determined based on density functional theory calculations, which revealed the existence of a multi-center double bond between the two norcorrole macrocycles. The binding electron density was experimentally determined using a synchrotron X-ray diffraction analysis. Our experimental demonstration of the existence of this intermolecular double bond can be expected to stimulate the search for intermolecular triple and even higher-order multiple bonds in other π-conjugated organic molecules.

References

(1) Thakuria, R., Nath, N. K. & Saha, B. K. The Nature and Applications of π–π Interactions: A Perspective. *Cryst. Growth Des.* **19**, 523–528 (2019).

(2) Pérez, E. M. & Martín, N. π–π interactions in carbon nanostructures. *Chem. Soc. Rev.* **44**, 6425–6433 (2015).

(3) Chen, Z., Lohr, A., Saha-Möller, C. R. & Würthner, F. Self-assembled π-stacks of functional dyes in solution: structural and thermodynamic features. *Chem. Soc. Rev.* **38**, 564–584 (2009).

(4) McGaughey, G. B., Gagné, M. & Rappé, A. K. π-Stacking Interactions. *J. Biol. Chem.* **273**, 15458–15463 (1998).

(5) Iwane, M. *et al.* Controlling stacking order and charge transport in π-stacks of aromatic molecules based on surface assembly. *Chem. Commun.* **54**, 12443–12446 (2018).

(6) Martinez, C. R. & Iverson, B. L. Rethinking the term "pi-stacking". *Chem. Sci.* **3**, 2191 (2012).

(7) Grimme, S. Do Special Noncovalent π–π Stacking Interactions Really Exist? *Angew. Chem., Int. Ed.* **47**, 3430–3434 (2008).

(8) Janiak, C. A critical account on π–π stacking in metal complexes with aromatic nitrogen-containing ligands. *J. Chem. Soc., Dalton Trans.* 3885–3896 (2000).

(9) Goto, K. *et al.* A Stable Neutral Hydrocarbon Radical: Synthesis, Crystal Structure, and Physical Properties of 2,5,8-Tri-*tert*-butyl-phenalenyl. *J. Am. Chem. Soc.* **121**, 1619–1620 (1999).

(10) Xiang, Q. *et al.* Stable Olympicenyl Radicals and Their π-Dimers. *J. Am. Chem. Soc.* **142**, 11022–11031 (2020).

(11) Jiao, T. *et al.* Synthesis of monolayer and persistent bilayer graphene fragments by using a radical-mediated coupling approach. *Nat. Synth.* 1–12 (2023) doi:10.1038/s44160-023-00348-w.

(12) Morita, Y. *et al.* Organic tailored batteries materials using stable open-shell molecules with degenerate frontier orbitals. *Nat. Mater.* **10**, 947–951 (2011).

(13) Ikabata, Y. *et al.* Near-infrared absorption of π-stacking columns composed of trioxotriangulene neutral radicals. *npj Quantum Mater.* **2**, 1–7 (2017).

(14) Mulliken, R. S. & Person, W. B. Molecular Complexes; Wiley & Sons: 1969; Chapter 16.

(15) Preuss, K. E. Pancake bonds: π-Stacked dimers of organic and light-atom radicals. *Polyhedron* **79**, 1–15 (2014).

(16) Kertesz, M. Pancake Bonding: An Unusual Pi-Stacking Interaction. *Chem.-Eur. J.* **25**, 400–416 (2019).

(17) Miller, J. S. Four-Center Carbon−Carbon Bonding. *Acc. Chem. Res.* **40**, 189–196 (2007).

(18) Cui, Z., Lischka, H., Beneberu, H. Z. & Kertesz, M. Double Pancake Bonds: Pushing the Limits of Strong π–π Stacking Interactions. *J. Am. Chem. Soc.* **136**, 12958–12965 (2014).

(19) Mou, Z. & Kertesz, M. Pancake Bond Orders of a Series of π-Stacked Triangulene Radicals. *Angew. Chem., Int. Ed.* **56**, 10188–10191 (2017).

(20) Corminboeuf, C., Schleyer, P. v. R. & Warner, P. Are antiaromatic rings stacked face-to-face aromatic? *Org. Lett.* **9**, 3263-3266 (2007).

(21) Bean, D. E. & Fowler, P. W. Stacked-ring aromaticity: an orbital model. *Org. Lett.* **10**, 5573-5576 (2008).

(22) Aihara, J. Origin of Stacked-Ring Aromaticity. *J. Phys. Chem. A* **113**, 7945–7952 (2009).

(23) Okazawa, K., Tsuji, Y. & Yoshizawa, K. Frontier Orbital Views of Stacked Aromaticity. *J. Phys. Chem. A* **127**, 4780–4786 (2023).

(24) Tsuji, Y., Okazawa, K. & Yoshizawa, K. Hückel Molecular Orbital Analysis for Stability and Instability of Stacked Aromatic and Stacked Antiaromatic Systems. *J. Org. Chem.* (2023) doi:10.1021/acs.joc.3c01167.

(25) Nozawa, R. *et al.* Stacked antiaromatic porphyrins. *Nat. Commun.* **7**, 13620 (2016).

(26) Nozawa, R. *et al.* Three-dimensional aromaticity in an antiaromatic cyclophane. *Nat. Commun.* **10**, 3576 (2019).

(27) Kawashima, H. *et al.* Determinant Factors of Three-Dimensional Aromaticity in Antiaromatic Cyclophanes. *J. Am. Chem. Soc.* **143**, 10676–10685 (2021).

(28) Ito, T. *et al*. Gram-scale synthesis of nickel(II) norcorrole: the smallest antiaromatic porphyrinoid. *Angew. Chem., Int. Ed.* **51**, 8542-8545 (2012).

(29) Krygowski, T. M. & Cyrański, M. K. Structural Aspects of Aromaticity. *Chem. Rev.* **101**, 1385–1420 (2001). Krygowski, T. M. & Cyrański, M. K. Structural Aspects of Aromaticity. *Chem. Rev.* **101**, 1385–1420 (2001).

(30) Becke, A. D. Density-functional thermochemistry. III. The role of exact exchange, *J. Chem. Phys*. **98**, 5648–5652 (1993).

(31) Weigend, F. & Ahlrichs, R. Balanced basis sets of split valence, triple zeta valence and quadruple zeta valence quality for H to Rn: Design and assessment of accuracy. *Phys. Chem. Chem. Phys.* **7**, 3297–3305 (2005).

(32) Grimme, S., Ehrlich, S. & Goerigk, L. Effect of the damping function in dispersion corrected density functional theory. *J. Comput. Chem.* **32**, 1456–1465 (2011).

(33) Bader, R. F. W. A quantum theory of molecular structure and its applications. *Chem. Rev.* **91**, 893–928 (1991).

(34) Lu, T. & Chen, F. Multiwfn: A multifunctional wavefunction analyzer. *J. Comput. Chem.* **33**, 580–592 (2012).

(35) Espinosa, E., Molins, E. & Lecomte, C. Hydrogen bond strengths revealed by topological analyses of experimentally observed electron densities. *Chem. Phys. Lett.* **285**, 170–173 (1998).

(36) Casida, M. E. & Huix-Rotllant, M. Progress in Time-Dependent Density-Functional Theory. *Annu. Rev. Phys. Chem.* **63**, 287–323 (2012).

(37) Yanai, T., Tew, D. P. & Handy, N. C. A new hybrid exchange–correlation functional using the Coulomb-attenuating method (CAM-B3LYP). *Chem. Phys. Lett.* **393**, 51–57 (2004).

(38) Becke, A. D. A new mixing of Hartree–Fock and local density-functional theories. *J. Chem. Phys.* **98**, 1372–1377 (1993).

(39) Lehtola, S., Steigemann, C., Oliveira, M. J. T. & Marques, M. A. L. Recent developments in libxc – A comprehensive library of functionals for density functional theory. *SoftwareX* **7**, 1–5 (2018).

(40) Jusélius, J., Sundholm, D. & Gauss, J. Calculation of current densities using gauge-including atomic orbitals. *J. Chem. Phys.* **121**, 3952–3963 (2004).

(41) Fliegl, H., Taubert, S., Lehtonen, O. & Sundholm, D. The gauge including magnetically induced current method. *Phys. Chem. Chem. Phys.* **13**, 20500–20518 (2011).

(42) Sundholm, D., Fliegl, H. & Berger, R. J. F. Calculations of magnetically induced current densities: theory and applications. *Wiley Interdiscip. Rev. Comput. Mol. Sci.* **6**, 639–678

(2016).
(43) Sundholm, D., Dimitrova, M. & Berger, R. J. F. Current density and molecular magnetic properties. *Chem. Commun.* **57**, 12362–12378 (2021).
(44) The GIMIC program is freely available at https://github.com/qmcurrents/gimic and https://zenodo.org/record/8180435.
(45) Ahrens, J., Geveci, B. & Law, C. ParaView: An End-User Tool for Large-Data Visualization. in *Visualization Handbook* (eds. Hansen, C. D. & Johnson, C. R.) 717–731 (Butterworth-Heinemann, 2005).
(46) Ditchfield, R. Self-consistent perturbation theory of diamagnetism. *Mol. Phys.* **27**, 789–807 (1974).
(47) Wolinski, K., Hinton, J. F. & Pulay, P. Efficient implementation of the gauge-independent atomic orbital method for NMR chemical shift calculations. *J. Am. Chem. Soc.* **112**, 8251–8260 (1990).
(48) Wang, Q., Pyykkö, J., Dimitrova, M., Taubert, S. & Sundholm, D. Current-density pathways in figure-eight-shaped octaphyrins. *Phys. Chem. Chem. Phys.* **25**, 12469–12478 (2023).
(49) Schleyer, P. von R., Maerker, C., Dransfeld, A., Jiao, H. & van Eikema Hommes, N. J. R. Nucleus-Independent Chemical Shifts: A Simple and Efficient Aromaticity Probe. *J. Am. Chem. Soc.* **118**, 6317–6318 (1996).
(50) Platt, J. R. Classification of Spectra of Cata-Condensed Hydrocarbons. *J. Chem. Phys.* **17**, 484–495 (1949).
(51) Waluk, J. & Michl, J. Perimeter model and magnetic circular dichroism of porphyrin analogs. *J. Org. Chem.* **56**, 2729–2735 (1991).

Data availability

Crystallographic data (CIF file) for **1** have been deposited with the Cambridge Crystallographic Data Centre as supplementary publications. CCDC-2301838 contains the supplementary crystallographic data. These data can be obtained free of charge from the Cambridge Crystallographic Data Centre via [www.ccdc.cam.ac.uk/data_request/cif]. All other data supporting the findings of this study are available within the article and its Supplementary Information.

Acknowledgements

This work was supported by JSPS KAKENHI grants JP20H05862, JP20H05863, JP20H05867,

JP22H04974, and JP22K19025. The synchrotron X-ray study was performed with the approval of the Photon Factory Program Advisory Committee (proposal 2020S2-001). S.U. is grateful to a JSPS Research Fellowship for Young Scientists (JP20J11883). This work has also been supported by the Academy of Finland (340583). Q.W. thanks the China Scholarship Council for a pre-doctoral fellowship. Computational resources from the CSC–IT Center for Science (Finland) are also acknowledged.

Author contributions

S.K. and S.U. contributed equally to this manuscript. H.S., R.K., and D.S. designed and conducted the project and prepared the manuscript. S.U. synthesized and characterized **1** and S.K. investigated its structure and properties in the solid state and in solution. F.N. and R.H. carried out the X-ray diffraction analysis. S.H. measured the solid-state NMR spectra. Q.M.P. and Q.W. carried out the theoretical studies.

Competing interests

The authors declare no competing interests.